Comparison of Basic Inductive Power Transfer Systems With Linear Control Achieving Optimized Efficiency

Zhicong Huang ⬡, *Member, IEEE*, Siu-Chung Wong ⬡, *Senior Member, IEEE*, and Chi K. Tse, *Fellow, IEEE*

Abstract—**Inductive power transfer (IPT) systems with front-side and load-side converters are generally developed for better overall system efficiency than a single IPT converter by providing maximum efficiency tracking and output regulation against variations of coupling coefficient (k) and load. The optimum efficiency point of an IPT converter is at a particular loading resistance, which varies with k and is hard to measure directly for the purpose of control. Perturb and observe control is normally implemented to iteratively track the optimum efficiency point. However, this heuristic algorithm results in slow response to the variations of k and load. Recently, a much faster linear control for optimum efficiency tracking has been developed for the series-series (SS) IPT system only. This paper proposes a general linear control scheme for all four basic IPT systems to track the optimum efficiency point. Unlike the SS IPT converter, it is found that additional control of either frequency or adaptive compensation is needed for the other three basic IPT converters to operate against the variation of k. Different input to output transfer functions and their k- and load-independent properties at optimum efficiency are identified for all four basic IPT systems. Thus, a general fast linear control can be applied in the front-side converter to achieve optimum efficiency, while the load-side converter regulates the output power independently. Furthermore, the maximum efficiencies of the IPT converters with these four basic compensations for an identical loosely-coupled transformer are compared theoretically and verified experimentally. The parallel–parallel IPT converter gives the best efficiency. Its additional frequency control in conjunction with the optimum efficiency tracking and the output power regulation is also experimentally validated.**

Index Terms—**Comparison, inductive power transfer (IPT), linear control, optimized efficiency.**

I. INTRODUCTION

INDUCTIVE power transfer (IPT) systems have found many applications in wireless charging of portable electronic devices [1]–[4], roadway-powered electric vehicles [5]–[9], and biomedical implants [10]–[12]. IPT converters inevitably contain loosely-coupled transformers in order to allow power to be transmitted wirelessly between the primary and secondary windings. The large leakage inductance of the transformer must be compensated using external capacitors and/or inductors in order to achieve near zero reactive power so that the power rating and loss from the power driver can be substantially minimized [13], [14]. The basic IPT converters contain minimal number of external compensation components, i.e., two capacitors, one at each side of the transformer windings. The connections can be in series or parallel. Thus, four basic IPT converters can be identified according to the primary–secondary compensation types, namely, series–series (SS), series–parallel (SP), parallel–series (PS), and parallel–parallel (PP) IPT converters. Once compensated, an IPT converter behaves as a resonant converter with the maximum efficiency occurring at a very narrow vicinity of an optimal operating point [15]. When the operating point deviates slightly from the optimal point, the converter efficiency drops significantly.

To maintain the IPT converter at its optimal operating point for applications with large variations of coupling coefficient (k) and load, maximum efficiency tracking (MET) has been widely studied. In [16], a load-side converter cascaded to an SS IPT converter is used to adaptively emulate an optimal load. However, no regulation of the load power is provided by the load-side converter. Improved IPT systems with MET algorithms have been proposed. The improved system has a front-side converter (or the internal inverter of the IPT converter) controlled to maximize the efficiency (or minimize the input power), while the load-side converter is responsible for the regulation of the output power against load change [17]–[23].

Typical MET algorithms are based on an iterative computer algorithm called "perturb and observe" (P&O) [16]–[23]. The P&O algorithm inevitably has to balance between a sufficiently small steady-state error and an acceptable dynamic response by choosing a suitable incremental value of the control variable. In these IPT systems, the slow iterative process of the P&O algorithm often results in poor dynamic response to the variations of k and load. Furthermore, it may cause large

overshoot/undershoot due to some seriously-mismatched-load conditions during the iterative process. In [22], with an improved sliding mode controller, the load-side converter is more adaptive to the slow response of the iterative process of P&O. However, IPT systems with P&O and sliding mode control, to a less extent, still suffer from seriously-mismatched-load conditions. Since the maximum efficiency point occurs at a specific value of the modulation index for controlling the power of the IPT converter, an iterative algorithm for MET is still a necessity. Nonetheless, a noniterative controller is desired. Fortunately, maximum efficiency is found to be at a specific voltage transfer ratio of the SS IPT converter designed at its optimal operating point with a load-independent transconductance and an input zero phase angle (ZPA) such that the relationship between the modulation index and the voltage transfer ratio is monotonic, thus allowing a linear controller to be developed [24]. The linear controller for the SS IPT converter has been proved to have a much faster response and smaller steady-state error in keeping the system at its maximum efficiency against the variations of k and load. However, the linear maximum efficiency controller is only available for SS IPT systems. Linear controllers for maximum efficiency operation of all four basic IPT converters and their efficiency comparisons are still missing.

In this paper, conditions for achieving load-independent transfer function and ZPA will be highlighted for all four basic IPT converters. Additional requirements of frequency or compensation control are illustrated for the optimum operations of SP, PS, and PP IPT converters against variation of k. Control references of transfer functions at maximum efficiency points of these IPT converters are derived for maximum efficiency control. The linear control scheme proposed in [24] can therefore be applied in these IPT systems for achieving efficiency optimization against the variations of k and load. A comparison of maximum achievable efficiency for these four basic IPT converters taking into consideration losses from practical converters will be given. This paper presents a generalization of the research work in [24] to cover all basic IPT converter systems.

This paper is organized as follows. Section II introduces the four basic IPT converters and derives the optimum operating points for achieving load-independent output, maximum efficiency, and ZPA. In Section III, control references at the optimum operating points are derived for the linear controllers. Section IV compares power efficiencies of practical systems using the four basic compensations. Section V elaborates the linear control scheme for achieving maximum efficiency with output regulation against the variation of k. Experimental verifications are given in Section VI. Finally, Section VII concludes this paper.

II. Optimal Efficiency Operating Point of an IPT Converter Model

A. Basic IPT Converter

Fig. 1 shows some essential building blocks of a basic IPT converter model, where the loosely-coupled transformer has self inductances L_P and L_S, and a mutual inductance M. As usual, the coupling coefficient k is defined as $\frac{M}{\sqrt{L_P L_S}}$. Unless indicated otherwise, subscripts P and S indicate parameters on the primary and secondary sides, respectively. Using this
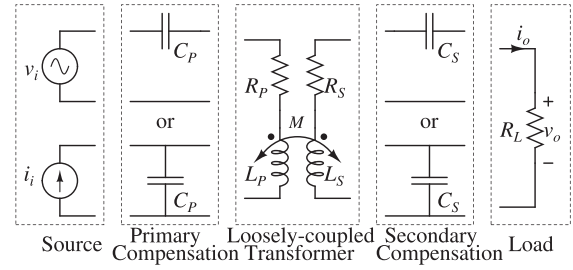

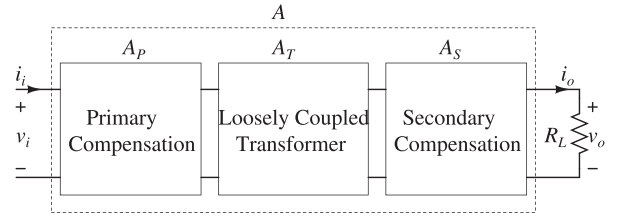Fig. 1. Essential building blocks of a basic IPT converter.

Fig. 2. Schematic of an IPT converter as a two-port network.

transformer model, losses are modeled aggregately using equivalent resistors R_P and R_S as described in [25], [26]. Resistor R_P includes losses from the primary windings and the inverter circuit. Resistor R_S includes losses from the secondary windings and the rectifier circuit. External capacitors C_P and C_S are used to compensate the loosely-coupled transformer in either series or parallel connection. They resonate with self inductances at frequencies $\omega_P = \frac{1}{\sqrt{L_P C_P}}$ and $\omega_S = \frac{1}{\sqrt{L_S C_S}}$. For an appropriate primary-side compensation, an IPT converter with primary series compensation is mostly driven by an equivalent ac voltage source v_i, while an IPT converter with primary parallel compensation is mostly driven by an equivalent ac current source i_i. Normally, either output voltage v_o or output current i_o is regulated conveniently for the required output power. In this way, we can have two output transfer functions for each type of power source. For voltage input, the transfer functions are a voltage gain $\frac{v_o}{v_i}$ and a transconductance $\frac{i_o}{v_i}$. Likewise, for current input, the transfer functions are a transresistance $\frac{v_o}{i_i}$ and a current gain $\frac{i_o}{i_i}$. The power regulation for MET will need the control of both transfer functions. It can be enhanced by designing one of the two transfer functions to achieve a load-independent output. With this load-independent design, the two transfer functions are polarized and targeting to be either completely load-independent or completely load-dependent.

B. Two-Port Network Model

The schematics of IPT converters shown in Fig. 1 can be simplified using two-port networks [27], as shown in Fig. 2. The two-port networks are represented by

$$[v_i, i_i]^T = A[v_o, i_o]^T \tag{1}$$

where $A = A_P A_T A_S$ is the product of the gains of primary compensation A_P, loosely-coupled transformer A_T, and secondary compensation A_S. The details of subnetworks are given in Table I. As two-port network A only consists of linear passive

TABLE I
MATRIX OF SUBNETWORKS

	Series Compensation	Parallel Compensation
A_P	$\begin{bmatrix} 1 & \frac{1}{j\omega C_P} \\ 0 & 1 \end{bmatrix}$	$\begin{bmatrix} 1 & 0 \\ j\omega C_P & 1 \end{bmatrix}$
A_S	$\begin{bmatrix} 1 & \frac{1}{j\omega C_S} \\ 0 & 1 \end{bmatrix}$	$\begin{bmatrix} 1 & 0 \\ j\omega C_S & 1 \end{bmatrix}$
A_T	$\begin{bmatrix} \frac{j\omega L_P + R_P}{j\omega M} & j\omega M(\frac{1}{k^2}-1) + \frac{R_P R_S + j\omega L_P R_S + j\omega L_S R_P}{j\omega M} \\ \frac{1}{j\omega M} & \frac{j\omega L_S + R_S}{j\omega M} \end{bmatrix}$	

inductors, capacitors, and parasitic resistors, it is a reciprocal network. Define

$$A = \begin{bmatrix} a_{11} & a_{12} \\ a_{21} & a_{22} \end{bmatrix} \quad (2)$$

and by the principle of reciprocity, we have

$$a_{11}a_{22} - a_{12}a_{21} = 1 \quad (3)$$

and

$$\begin{bmatrix} v_i \\ i_i \end{bmatrix} = A \begin{bmatrix} v_o \\ i_o \end{bmatrix} = \begin{bmatrix} a_{11} & a_{12} \\ a_{21} & a_{22} \end{bmatrix} \begin{bmatrix} v_o \\ i_o \end{bmatrix}. \quad (4)$$

Obviously, from Fig. 2, we also have $v_o = i_o R_L$.

Load-independent transfer functions have been studied previously for the SS, SP, and PP IPT converters [25], [26], [28]. It is found that for an efficiency-optimized design, the SS and PS IPT converters should achieve load-independent current output while the SP and PP IPT converters should achieve load-independent voltage (LIV) output. From (3) and (4), the transfer functions of the four IPT converters are readily given by

$$G = \begin{cases} \dfrac{i_o}{v_i} = \dfrac{1}{a_{11}R_L + a_{12}}, & \text{for SS} \quad (5a) \\[2mm] \dfrac{v_o}{v_i} = \dfrac{1}{a_{11} + \dfrac{a_{12}}{R_L}}, & \text{for SP} \quad (5b) \\[2mm] \dfrac{i_o}{i_i} = \dfrac{1}{a_{21}R_L + a_{22}}, & \text{for PS, and} \quad (5c) \\[2mm] \dfrac{v_o}{i_i} = \dfrac{1}{a_{21} + \dfrac{a_{22}}{R_L}} & \text{for PP} \quad (5d) \end{cases}$$

IPT converters. The conditions of load-independent outputs for SS, SP, PS, and PP IPT converters are $a_{11} = 0$ in (5a), $a_{12} = 0$ in (5b), $a_{21} = 0$ in (5c) and $a_{22} = 0$ in (5d), respectively.

From (4), the input impedance of these IPT converters is given by

$$Z_{\text{in}} = \frac{v_i}{i_i} = \frac{a_{11}R_L + a_{12}}{a_{12}R_L + a_{22}}. \quad (6)$$

To achieve ZPA between v_i and i_i, Z_{in} should have no imaginary component, i.e.,

$$\Re(Z_{\text{in}}) = Z_{\text{in}}. \quad (7)$$

In this paper, $\Re$ and $\Im$ represent the calculation of real component and imaginary component, respectively.

The power efficiency of the four IPT converters can be calculated from

$$\eta = \frac{\Re(v_o i_o)}{\Re(v_i i_i)}. \quad (8)$$

Table II gives a summary of expressions before optimization of transfer function G, input impedance Z_{in}, and efficiency η for the four basic IPT converters. These expressions will be optimized at an operating frequency for the desired load-independent transfer function and input ZPA.

C. Load-Independent Transfer Functions With ZPA

For a practical IPT converter, R_P and R_S are nonzero and thus a perfect load-independent transfer function is not possible. However, a near perfect load-independent transfer function can be obtained by assuming $R_P = 0$ and $R_S = 0$. With the conditions to achieve load-independent output and ZPA discussed in Section II-B [25], [26], [28], ideal load-independent transfer function $|G_i|$ is given by

$$|G_i| \approx \begin{cases} \left| \dfrac{i_o}{v_i} \right| = \dfrac{1}{\omega_P M}, & \text{for SS} \quad (9a) \\[2mm] \left| \dfrac{v_o}{v_i} \right| = \dfrac{L_S}{M}, & \text{for SP} \quad (9b) \\[2mm] \left| \dfrac{i_o}{i_i} \right| = \dfrac{L_P}{M}, & \text{for PS} \quad (9c) \\[2mm] \left| \dfrac{v_o}{i_i} \right| = \omega_S M \dfrac{\sqrt{1-k^2}}{k^2} & \text{for PP} \quad (9d) \end{cases}$$

compensated IPT converters, at an operating frequency ω, given by

$$\omega = \begin{cases} \omega_P = \omega_S, & \text{for SS} \quad (10a) \\[2mm] \omega_S = \dfrac{\omega_P}{\sqrt{1-k^2}}, & \text{for SP} \quad (10b) \\[2mm] \omega_P = \dfrac{\omega_S}{\sqrt{1-k^2}}, & \text{for PS} \quad (10c) \\[2mm] \dfrac{\omega_P}{\sqrt{1-k^2}} = \dfrac{\omega_S}{\sqrt{1-k^2}}, & \text{for PP} \quad (10d) \end{cases}$$

compensated IPT converters. From (10), ω, ω_P, or ω_S may vary with k as a consequence of misalignment or variation of the gap distance of the loosely coupled transformer. Thus, frequency control is needed for PP IPT converter and adaptive compensation is needed for SP and PS IPT converters to satisfy (10) when k varies. A summary is shown in Table III.

D. Optimal Load

The expressions of η in Table II are obtained by omitting the small equivalent series resistance of the compensation capacitors. The optimal loading resistance $R_{L,m}$ that achieves maximum efficiency can be obtained by putting ω from (10) into η in Table II, and solving $\frac{d\eta}{dR_L} = 0$ for $R_{L,m}$ which is

TABLE II
EXPRESSIONS OF TRANSFER FUNCTIONS, INPUT IMPEDANCE, AND EFFICIENCY

Topologies	G	Z_{in}	η
SS	$\frac{i_o}{v_i} = \frac{j\omega M}{Z_P Z_{S-S} + \omega^2 M^2}$	$Z_P + \frac{\omega^2 M^2}{Z_{S-S}}$	$\frac{\omega^2 M^2 R_L}{\lvert Z_{S-S}\rvert^2 R_P + \omega^2 M^2 (R_L + R_S)}$
PS	$\frac{i_o}{i_i} = \frac{\frac{M}{C_P}}{Z_P Z_{S-S} + \omega^2 M^2}$	$\frac{Z_P - \frac{1}{j\omega C_P} + \frac{\omega^2 M^2}{Z_{S-S}}}{j\omega C_P (Z_P + \frac{\omega^2 M^2}{Z_{S-S}})}$	
SP	$\frac{v_o}{v_i} = \frac{j\omega M \frac{R_L}{j\omega C_S R_L + 1}}{Z_P Z_{S-P} + \omega^2 M^2}$	$Z_P + \frac{\omega^2 M^2}{Z_{S-P}}$	$\frac{\omega^2 M^2 \frac{R_L}{1 + \omega^2 C_S^2 R_L^2}}{\lvert Z_{S-P}\rvert^2 R_P + \omega^2 M^2 (\frac{R_L}{1 + \omega^2 C_S^2 R_L^2} + R_S)}$
PP	$\frac{v_o}{i_i} = \frac{\frac{M}{C_P} \frac{R_L}{j\omega C_S R_L + 1}}{Z_P Z_{S-P} + \omega^2 M^2}$	$\frac{Z_P - \frac{1}{j\omega C_P} + \frac{\omega^2 M^2}{Z_{S-P}}}{j\omega C_P (Z_P + \frac{\omega^2 M^2}{Z_{S-P}})}$	
$Z_P = j\omega L_P + R_P + \frac{1}{j\omega C_P}$, $Z_{S-S} = j\omega L_S + R_S + \frac{1}{j\omega C_S} + R_L$ and $Z_{S-P} = j\omega L_S + R_S + \frac{R_L}{j\omega C_S R_L + 1}$.			

TABLE III
ADDITIONAL CONTROL REQUIREMENT FOR THE VARIATION OF k

Topologies	Adaptive Compensation	Frequency Tracking
SS	Nil	Nil
SP	Required	Nil
PS	Required	Nil
PP	Nil	Required

approximately given by

$$R_{L,m} \approx \begin{cases} \omega_P M \gamma, & \text{for SS} \quad (11a) \\ \\ \omega_S M \frac{L_S^2}{M^2} \frac{1}{\gamma}, & \text{for SP} \quad (11b) \\ \\ \omega_P M \gamma, & \text{for PS} \quad (11c) \\ \\ \omega_S M \sqrt{1 - k^2} \frac{L_S^2}{M^2} \frac{1}{\gamma}, & \text{for PP} \quad (11d) \end{cases}$$

compensated IPT converters, where

$$\gamma = \sqrt{\frac{R_S}{R_P}} \tag{12}$$

with assumptions

$$\frac{\omega^2 M^2}{R_P R_S} \gg 1 \tag{13}$$

$$\frac{1}{k^2} \gg \frac{L_P R_S}{L_S R_P} \gg k^2. \tag{14}$$

From (11), $R_{L,m}$ is k-dependent and difficult to be measured directly and accurately for operation at maximum efficiency. Therefore, a slow but universal P&O control algorithm is commonly used for the tracking of maximum efficiency or its equivalent directly.

III. k-INDEPENDENT MAXIMUM EFFICIENCY TRANSFER POINT

With the operating frequency given by (10), (9) gives the load-independent transfer function G_i, and (11) gives the load $R_{L,m}$ for optimal efficiency of the four basic IPT converters. As discussed in Section II-A, we have two transfer functions for the power control. The load-independent transfer function has been highlighted in Section II-C. The other transfer function should be load-dependent. It is defined as $H(R_L)$. At maximum efficiency point, we have $R_L = R_{L,m}$. Moreover, it is approximately

given by

$$H(R_{L,m}) \approx \begin{cases} \left\lvert \frac{v_o}{v_i} \right\rvert = \gamma, & \text{for SS} \quad (15a) \\ \\ \left\lvert \frac{i_o}{v_i} \right\rvert = \frac{1}{\omega_S L_S} \gamma, & \text{for SP} \quad (15b) \\ \\ \left\lvert \frac{v_o}{i_i} \right\rvert = \omega_P L_P \gamma, & \text{for PS and} \quad (15c) \\ \\ \left\lvert \frac{i_o}{i_i} \right\rvert = \frac{L_P}{L_S} \gamma, & \text{for PP} \quad (15d) \end{cases}$$

compensated IPT converters. Equation (15a) has been obtained previously in [24]. In this paper, it can be observed from (15) that $H(R_L)$ at $R_L = R_{L,m}$ is k- and load-independent for all four basic IPT converters. Therefore, it is possible to operate all basic IPT converters at maximum efficiency by controlling the output according to transfer function $H(R_{L,m})$, against the variations of k and load.

IV. COMPARISON OF MAXIMUM PRACTICAL EFFICIENCY OF THE FOUR BASIC IPT CONVERTERS

It is well known that the maximum efficiencies of the four basic IPT converters using the model shown in Fig. 1 are basically identical and increase with increasing k and the quality factors of the primary or secondary windings of the IPT transformer [15]. In this section, we will compare the maximum efficiency of the four basic IPT converters when the losses from the source-side inverter and the load-side diode rectifier are taken into consideration. Inverter loss includes conduction loss and switching loss. Switching loss can be minimized by zero voltage switching for MOSFET or zero current switching for IGBT inverter switches. Conduction loss increases with increasing current. For a given power level, higher resistance driving gives less loss for the inverter circuit. Output rectifier loss is mainly due to forward voltage drop. Therefore, higher rectifier loss is expected for higher rectifier current and lower output voltage. Similarly, higher resistance driving gives less loss for the diode-bridge circuit.

The input impedance at optimal load, defined as $Z_{\text{in,m}}$, can be calculated using (10) and (11). Since a small $\Im(Z_{\text{in,m}})$ is sufficient for soft switching, the inverter is mainly driving a
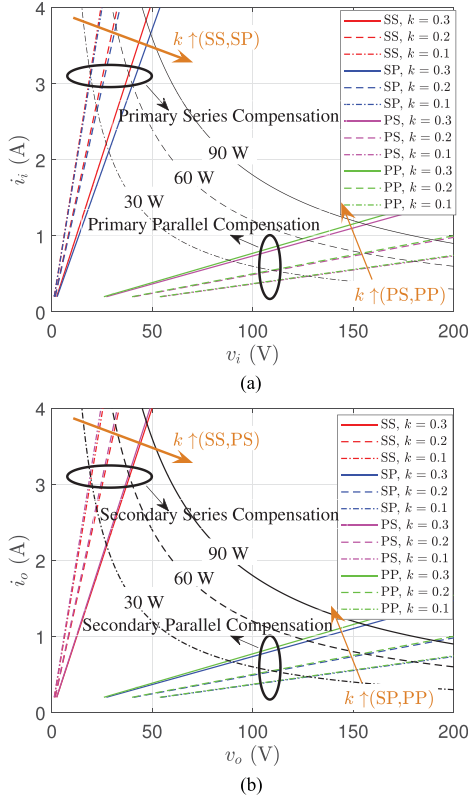
Fig. 3. V–I characteristics of SS, SP, PS, and PP IPT converters under different values of coupling coefficient k. The long arrows indicate the direction of line moving in response to an increase of k. (a) SS and SP IPT converters have a much higher inverter driving current. (b) SS and PS IPT converters have a much higher diode rectifier driving current.

resistive load with resistance given by

$$\Re(Z_{\text{in},m}) = \begin{cases} \omega_P M \dfrac{1}{\gamma} & \text{for SS,} & (16a) \\[2ex] \omega_P M \dfrac{1}{\gamma} \dfrac{1}{\sqrt{1-k^2}} & \text{for SP,} & (16b) \\[2ex] \omega_P M \gamma \dfrac{L_P^2}{M^2} & \text{for PS, and} & (16c) \\[2ex] \omega_P M \gamma \dfrac{L_P^2}{M^2} \sqrt{1-k^2} & \text{for PP} & (16d) \end{cases}$$

compensated IPT converters.

For illustration, simulations are conducted with parameters given as follows: $L_P = L_S = 120~\mu$H, $R_P = R_S = 0.5~\Omega$. A nominal frequency is defined as $\frac{\omega_{\text{nom}}}{2\pi} = 55$ kHz, $\omega = \omega_P = \omega_S = \omega_{\text{nom}}$ for the SS IPT converter, $\omega = \frac{\omega_P}{\sqrt{1-k^2}} = \omega_S = \omega_{\text{nom}}$ for the SP IPT converter, and $\omega = \omega_P = \frac{\omega_S}{\sqrt{1-k^2}} = \omega_{\text{nom}}$ for the PS IPT converter, and $\omega = \frac{\omega_P}{\sqrt{1-k^2}} = \frac{\omega_S}{\sqrt{1-k^2}} = \frac{\omega_{\text{nom}}}{\sqrt{1-k^2}}$ for the PP IPT converter. Unless specified otherwise, the parameters will be used for the rest of this paper.

According to the simulation parameters, the input and output V–I characteristics of the IPT converters are given in Fig. 3(a) and (b) by using (16) and (11), respectively. It can be observed that given a power, the current of parallel compensation of an IPT converter is much lower than that of series compensation. Thus, higher inverter and diode rectifier losses are expected for series compensated IPT converters. The losses are decreasing for series
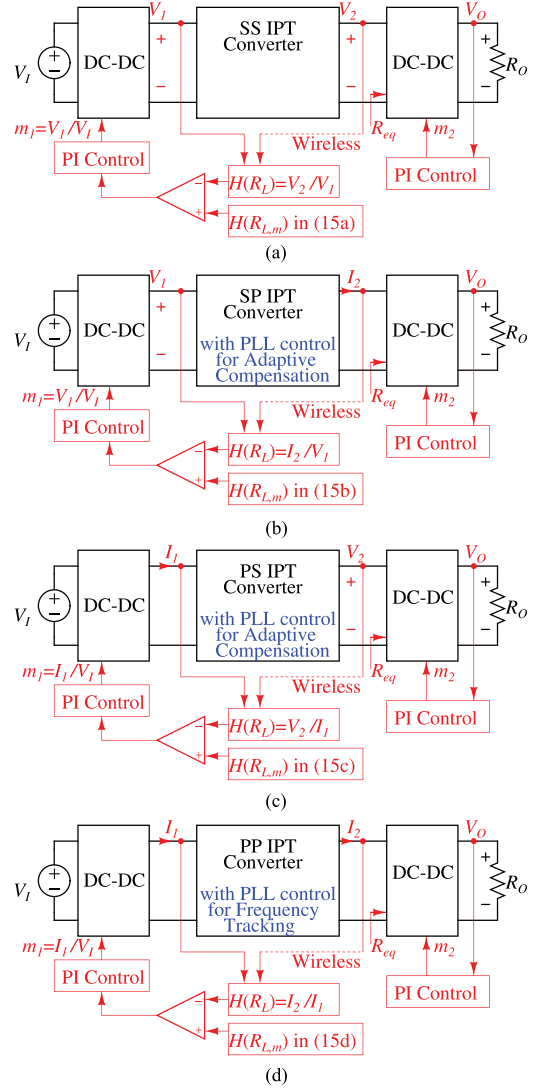

Fig. 4. Control diagrams of the three-stage IPT systems. (a) SS IPT system. (b) SP IPT system. (c) PS IPT system. (d) PP IPT system.

compensated windings but increasing for parallel compensated windings of the IPT converter with increasing k nevertheless. It is therefore expected that an IPT transformer compensated for the four basic IPT converters will have their own values of R_P and R_S described by the model as shown in Fig. 1.

V. CONTROL SCHEME

The IPT converters should be maintained at optimized efficiency according to (10) against the variation of k, and (11) against variation of load. To satisfy (10), frequency control and/or adaptive compensation may be needed within the IPT converter. Once (10) is satisfied, (9) and the inverter input ZPA will be automatically fulfilled for the easy implementation of linear control to satisfy (11). The extra control freedom offered by a multistage IPT system, as shown in Fig. 4, is often used for efficiency optimization in satisfying (11). The multistage IPT system includes a front-side dc–dc converter, an IPT converter, and a load-side dc–dc converter. In this paper, the load-side dc–dc converter is responsible for the regulation of output
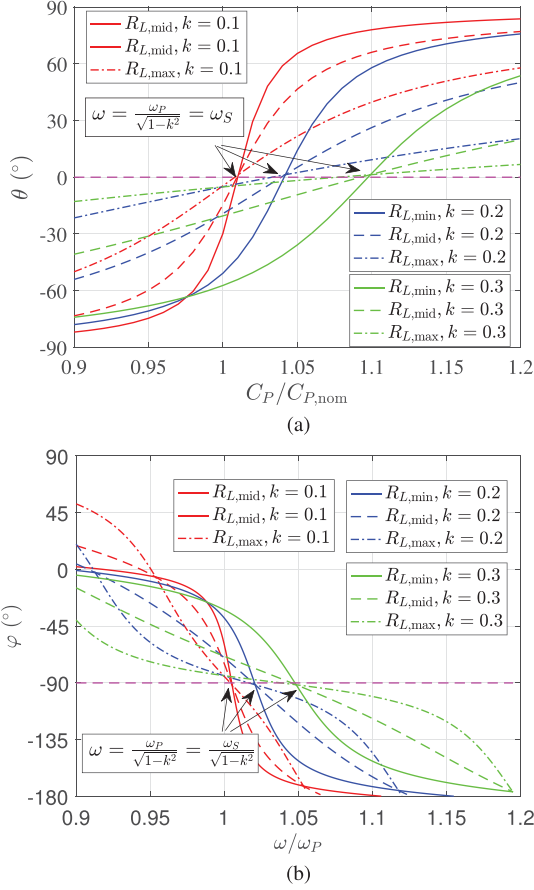
Fig. 5. (a) Input phase angle versus primary compensation capacitance of SP IPT converter. (b) Output phase angle versus operating frequency of PP IPT converter.

Fig. 6. Schematics of four IPT converters.

voltage V_O. The front-side dc–dc converter is responsible for achieving the load impedance given by (11).

A. Control for Adaptive Compensation and Frequency Tracking

To operate against the variation of k, control using adaptive compensation is needed for the SP and PS IPT converters, while control using frequency tracking is needed for the PP IPT converter as summarized in Table III of Section II-C. These controls can be implemented using the phase-locked loop (PLL)-based control in [29] and [30].

Simulation results of input phase angle defined as $\theta = \arctan\left(\Im(Z_{\text{in}})/\Re(Z_{\text{in}})\right)$ versus compensation capacitance of the SP IPT converter are shown in Fig. 5(a). When the SP IPT converter operates at conditions given in (10b), i.e., $\omega = \omega_S = \frac{\omega_P}{\sqrt{1-k^2}}$, θ is zero and independent of k. Moreover, θ has a monotonic relationship with the compensation capacitance C_P. Therefore, a PLL controller can be used to nullify the input phase angle by tuning the compensation capacitance. Compensation capacitance can be tuned by using a switching capacitor circuit [31]–[33]. Similar control scheme can also be implemented for the PS IPT converter.

In Fig. 5(b), $\varphi = \arctan\left(\Im(\frac{v_o}{i_i})/\Re(\frac{v_o}{i_i})\right)$ is the output phase angle between the secondary output voltage v_o and the primary input current i_i for the PP IPT converter. When the PP IPT
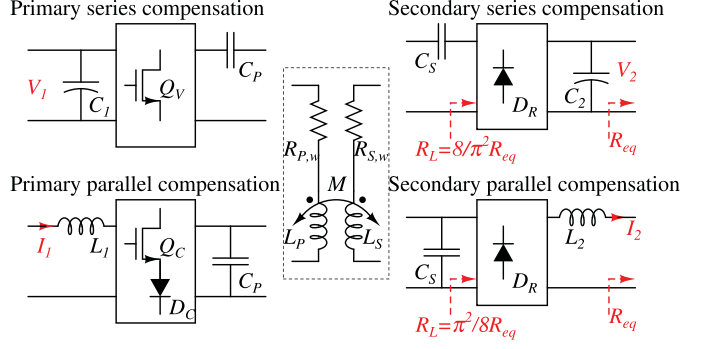
converter operates at condition (10d), φ is constant at $-90°$ and independent of k. Moreover, φ has a monotonic relationship with the operating angular frequency ω. Therefore, a PLL controller can be used for frequency tracking.

B. Control for Optimized Efficiency and Output Regulation

The load-side converter regulates the output voltage V_O, so that the load appears as a constant power load P_O at the output of the IPT converter. When using a front-side pulsewidth modulation converter, V_1 or I_1 is the modulated output of V_{IN} with modulation index m_1 given by $m_1 = \frac{V_1}{V_I}$ or $m_1 = \frac{I_1}{V_I}$. The equivalent load resistance R_L, as shown in Fig. 1, of the IPT converter is scaled from R_{eq} at the input of the load-side converter. Since the switching frequency of the resonant circuit is much higher than the variation speed of R_{eq}, which is controlled within a much lower bandwidth in the controller of the load-side converter, R_L is considered as a slowly varying dc resistor to the resonant circuit. The scaling factor is shown in Fig. 6. Since the input of the load-side converter is a near constant power sink, its input resistance can be adjusted by varying either load-independent output V_2 or I_2. By controlling m_1, R_L is controlled to its optimal value $R_{L,m}$. Thus, the IPT converters can achieve their maximum efficiencies.

Modulation index m_1 has been utilized by some P&O controllers to track the maximum efficiency point. However, the dynamic response of the controller can be slow against the variations of k or load, drifting R_{eq} far away from its optimal value. Therefore, the output voltage or current of the IPT converter can be significantly overshoot or undershoot in response to the variations of k or load. It is a challenge for the design and control of the load-side converter. It has shown in [24] that using a linear PI controller to track the maximum efficiency point has advantages of faster transient response and zero steady-state error against the variations of k and load. Therefore, this paper is a generalization of the technique presented in [24] for achieving optimized efficiency for all four basic IPT converters.

As an illustration, monotonic curves of transfer function $H(R_L)$ versus control variable m_1 for various values of k are shown in Fig. 7. We observe that when the IPT converter operates at its maximum efficiency, the value of $H(R_L)$ is constant at $H(R_{L,m})$. Therefore, transfer functions $H(R_{L,m})$ calculated at $R_{L,m}$ in (15) can be a control reference for achieving maximum power efficiency [24].
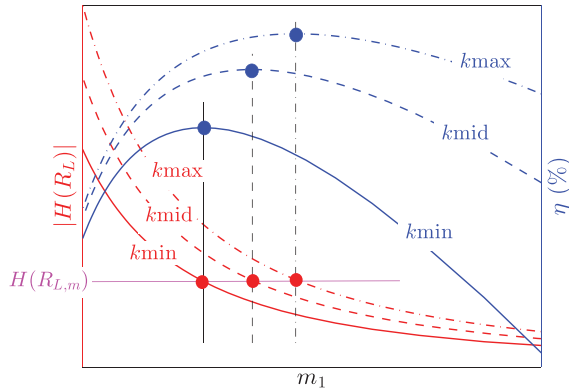
Fig. 7. Transfer function $H(R_L)$ and efficiency η versus control variable m_1.

TABLE IV
EXPERIMENTAL PARAMETERS OF FOUR IPT CONVERTERS

Inverter and Rectifier		
Parameters	Symbols	Values
Switch	Q_V, Q_C	IPP60R165CP
	D_C, D_R	MBRB2020CT
Filter	C_1, C_2	0.47 mF
	L_1, L_2	0.68 mH

Loosely-coupled transformer		
Parameters	Symbols	Values
Inner diameter	d_i	29 mm
Outer diameter	d_o	132 mm
Primary turn number	N_P	41
Secondary turn number	N_S	41
Primary self inductance	L_P	117.79 μH
Secondary self inductance	L_S	116.52 μH
Primary winding resistance	$R_{P,w}$	541.5 mΩ
Secondary winding resistance	$R_{S,w}$	535.2 mΩ
Air gap distance	g_1 (Position A)	36 mm
	g_2 (Position B)	52 mm
Coupling coefficient	k_1 (Position A)	0.28
	k_2 (Position B)	0.17

	Compensation and Operating Frequency					
	Parameters	Symbols	Values			
			SS	SP	PS	PP
k_1	Primary capacitance	C_P (nF)	78	84.4	78	78
	Secondary capacitance	C_S (nF)	78.2	78.2	86.1	78.2
	Operating frequency	f_{SW} (kHz)	52.6	52.6	52.6	54.79
k_2	Primary capacitance	C_P (nF)	78	80.1	78	78
	Secondary capacitance	C_S (nF)	78.2	78.2	81.1	78.2
	Operating frequency	f_{SW} (kHz)	52.6	52.6	52.6	53.39

Fig. 8. Experiment setup.

In practical applications, a dc input (voltage V_1 or current I_1) and a dc output (voltage V_2 or current I_2) are measured to generate the dc transfer function for feedback control according to the type of the IPT converter shown in Fig. 4. Wireless communication is necessary to transmit information of the dc output (voltage V_2 or current I_2). Neglecting higher order harmonics, the optimized dc transfer function is identical to the magnitude of ac transfer function. Therefore, $H(R_{L,m})$ in (15) is the control reference, as shown in Fig. 4. With proper design, simple linear PI controllers can be implemented in either analog or digital form, which results in a fast response, near zero steady-state error, simple structure, robust, and high reliability controller.

VI. EXPERIMENTAL VERIFICATION

To verify the maximum efficiency points and evaluate the efficiency performance of the basic IPT converters developed in this paper, prototypes of the four basic IPT converters using transformers with identical specifications are constructed. The circuit schematics are shown in Fig. 6, and detailed parameters of the components are given in Table IV. Two kinds of full bridge inverters with different switches are used to generate the ac voltage source and ac current source, for IPT converters with primary series compensation and parallel compensation, respectively [34], [35]. Rectifiers with C filter and L filter are used to convert ac to dc output for IPT converters with secondary series compensation and parallel compensation, respectively [34], [35].

The circular unipolar pad structure is selected to construct the loosely-coupled transformer as shown in Fig. 8. Parameters of the loosely-coupled transformer are given in Table IV. A dc motor is used to dynamically change the position of the secondary coupler between position A and B. At position A, the air gap distance g_1 is 36 mm and the coupling coefficient k_1 is 0.28. At position B, g_2 is 52 mm and the coupling coefficient k_2 is 0.17.

The compensation capacitors are tuned and the switching frequencies f_{SW} are adjusted to ensure that the IPT converters are operating at load-independent output with near ZPA input for soft-switching of inverter switches. The corresponding values of the compensation capacitors and the operating frequencies are also given in Table IV.
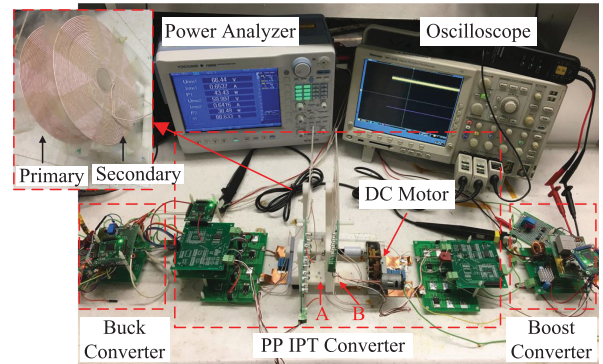
From (15), equivalent resistances R_P and R_S should be known to derive accurate optimized transfer functions for these IPT converters in order to achieve maximum efficiency. Apart from the winding loss in $R_{P,w}$ and $R_{S,w}$, additional inverter loss and additional rectifier loss should be incorporated into R_P and R_S, respectively. Therefore, optimized transfer functions can be calculated using circuit models with precise component parameters. Moreover, they can also be readily measured experimentally if the parameters are not available.

A. Transfer Function $H(R_L)$ at Maximum Efficiency Point

Efficiencies of the four IPT converters are measured at $k_1 = 0.28$ (position A) and $k_2 = 0.17$ (position B) by a Yokogawa
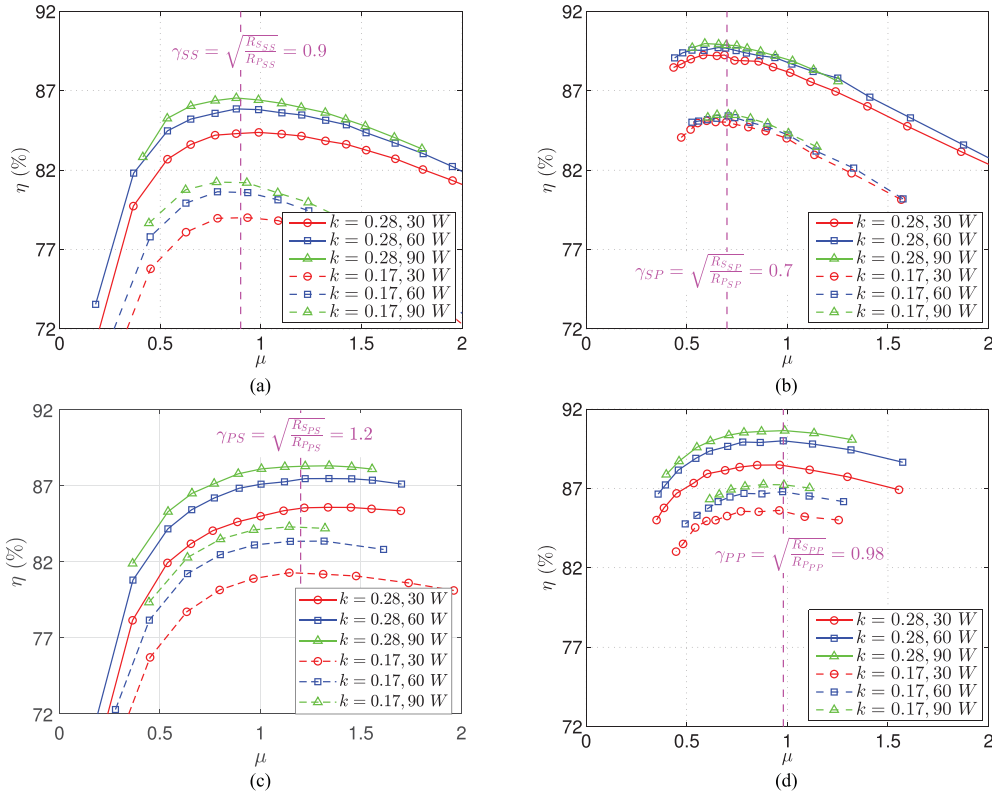
Fig. 9. Efficiency versus $\mu = \frac{\gamma H(R_L)}{H(R_{L,m})}$ for different values of coupling coefficient and load power. Vertical dash lines indicate the maximum efficiency points with a direct readout of γ. (a) SS. (b) SP. (c) PS. (d) PP.

PX8000 Precision Power Scope, including the losses from the inverter and the rectifier circuits. The output powers of the IPT converters are kept constant. By varying the input voltage or current of the IPT converters, efficiency curves versus a scaled $H(R_L)$ for different values of k and output power are measured and plotted as shown in Fig. 9.

From (15), the ratio $\frac{H(R_{L,m})}{\gamma}$ gives expressions of known parameters only, and the dimensionless parameter $\mu = \frac{\gamma H(R_L)}{H(R_{L,m})}$ gives a direct readout of γ at maximum efficiency point from a sequence of experimental data $H(R_L)$. It can be observed from the vertical dash line that near maximum efficiency can be achieved at a constant $H(R_L)$ identified for each IPT converter under different values of k and load. Therefore, these fixed value transfer functions can be used as control references for achieving maximum efficiency.

B. Comparison of Maximum Efficiency Points of the Four Basic IPT Converters

The comparison of maximum efficiency is based on the system illustrated in Fig. 4. The IPT transformer is designed and optimized under some physical constraints. This transformer is used for the four basic compensations for the determination of best efficiency.

From Fig. 9, the ratio after taking square is given by $(\frac{\gamma_{SS}}{\gamma_{PS}})^2 = \frac{R_{S_{SS}} R_{P_{PS}}}{R_{P_{SS}} R_{S_{PS}}}$, where $R_{S_{PS}}$ and $R_{S_{SS}}$ are roughly identical due to the same secondary circuitry. Thus, $\frac{R_{P_{PS}}}{R_{P_{SS}}} \approx (\frac{\gamma_{SS}}{\gamma_{PS}})^2 = 0.5625$. We may conclude that R_P of a primary parallel compensated

IPT converter is smaller than that of a primary series compensated IPT converter. Similarly, we have $R_{P_{PP}} \approx R_{P_{PS}}$ and $\frac{R_{S_{PP}}}{R_{S_{PS}}} \approx (\frac{\gamma_{PP}}{\gamma_{PS}})^2 = 0.6669$. Likewise, we may conclude that R_S of a secondary parallel compensated IPT converter is smaller than that of a secondary series compensated IPT converter. So, in general, parallel compensation has better efficiency than series compensation. Comparing maximum efficiencies at an identical power output of the SP and PS IPT converters, due to the lower output voltage of the PS IPT converter, the near constant diode drop loss is more significant at lower voltage output. Thus, the maximum efficiency of the SP IPT converter is better than the PS IPT converter. As a result, the maximum efficiency points are ordered from highest to lowest for IPT converters with compensations PP, PS, SP, and SS as shown in Fig. 9.

C. Input and Output Currents and Maximum Efficiency Points of the Four Basic IPT Converters

Fig. 10(a) and (b) shows the measured input current I_1 and the output current I_2 of the four basic IPT converters at maximum efficiency points. They agree with the analysis in Section IV, i.e., primary series compensation leads to a higher input current, and secondary series compensation leads to a higher output current at maximum efficiency point.

D. Control for Optimized Efficiency in PP IPT System

Optimal efficiencies at static conditions have been measured in Section VI-A for the four basic IPT converters. A simple
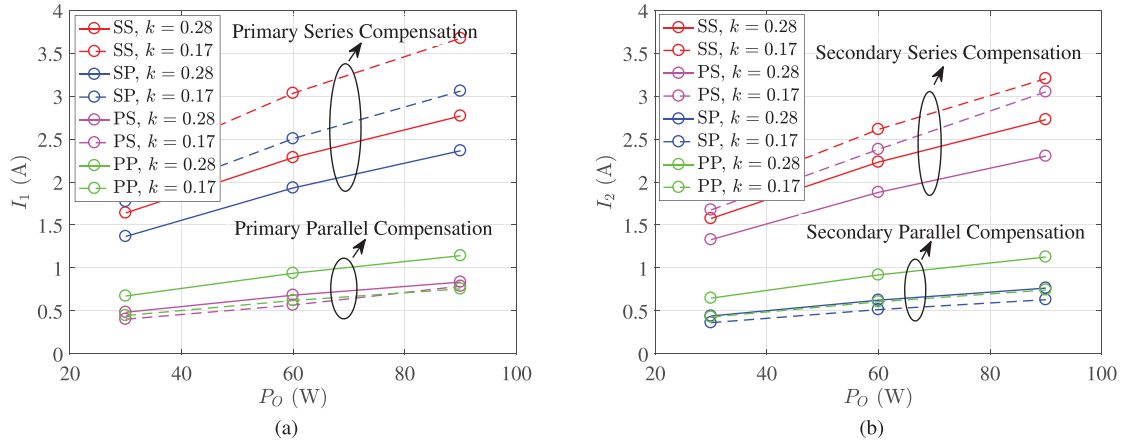
Fig. 10. (a) Measured input current I_1 and (b) measured output current I_2 of the four basic IPT converters at maximum power efficiency points.
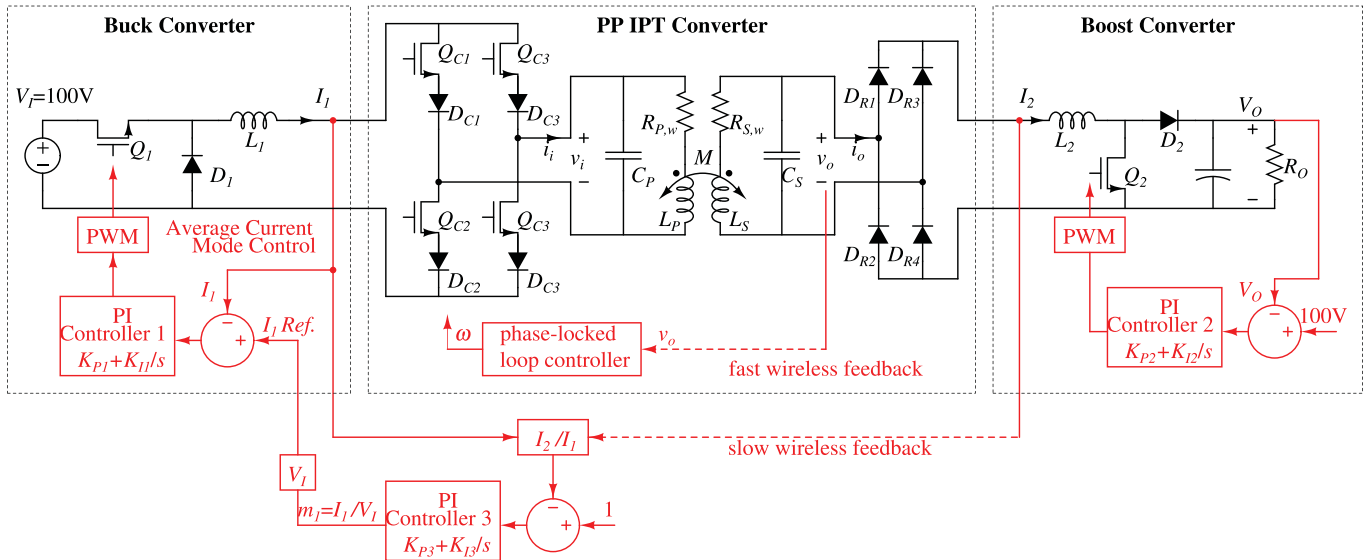

Fig. 11. Schematics and control diagrams of a multistage PP IPT system. Components: Q_1 and Q_2 are IPP60R165CP, D_1 and D_2 are MBRB2020CT. Parameters : $C_2 = 470\,\mu$F, $L_1 = L_2 = 3.3$ mH, $V_I = 100$ V, $V_O = 100$ V, $K_{P1} = 0.25$, $K_{I1} = 25$, $K_{P2} = 0.04$, $K_{I2} = 0.8$, $K_{P3} = 0.02$, $K_{I3} = 0.08$.

and fast control scheme has been developed for the SS IPT converter which does not need adaptive compensation and frequency tracking [24]. In Section VI-B, we have shown that the PP IPT converter has the highest efficiency. This converter is therefore selected in this paper for the experimental verification of the linear control scheme. A multistage system is constructed with schematics shown in Fig. 11, where the PP IPT converter is connected with a front-end buck converter and a load-side boost converter. A photo of the experimental setup is shown in Fig. 8.

Inside the PP IPT converter, the phase of ac voltage v_o is detected and transmitted wirelessly from the secondary to the primary via fast wireless feedback method, i.e., infrared emitter and receiver [29]. A PLL is implemented to control the operating frequency against the variation of k. Thus the PP IPT converter operates at LIV with ZPA and behaves as a transresistance

converter. For the front-end buck converter, current-mode control is used to program the inductor current which drives the PP IPT converter. The load-side boost converter is driven by the output voltage of the PP IPT converter and regulated by a standalone PI controller to generate a constant dc voltage output V_O. Currents I_1 and I_2 of the PP IPT converter are sampled. I_2 can be transmitted wirelessly from the secondary to the primary via a slow wireless feedback method, i.e., 2.4G. According to the experimental measurements shown in Fig. 9(d), $\frac{I_2}{I_1} \approx 1$ can be selected as control reference to achieve the optimized efficiency. A PI controller is used to control the transfer function $H(R_L) = \frac{I_2}{I_1}$.

With PLL control, the dynamic response of the operating frequency against the variation of k is recorded as shown in Fig. 12(a). Typical experimental waveforms of the PP IPT converter are shown in Fig. 12(b). Voltage v_o measured before the
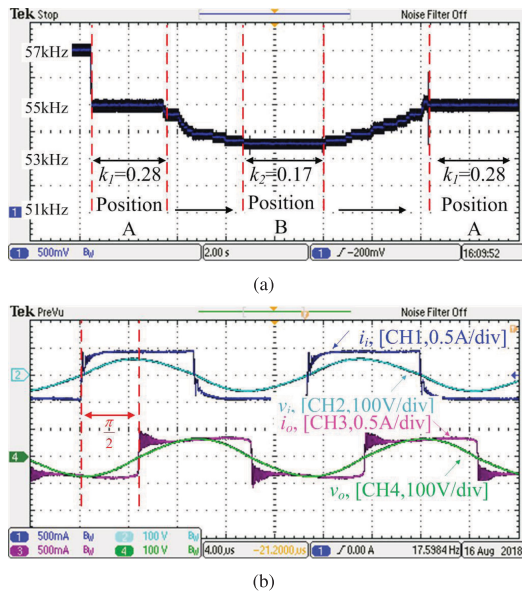
Fig. 12. (a) Reponse of the operating frequency when k dynamically changes from $k_1 = 0.28$ (position A) to $k_2 = 0.17$ (position B) and from $k_2 = 0.17$ (position B) back to $k_1 = 0.28$ (position A). (b) Experimental waveforms of PP IPT converter.
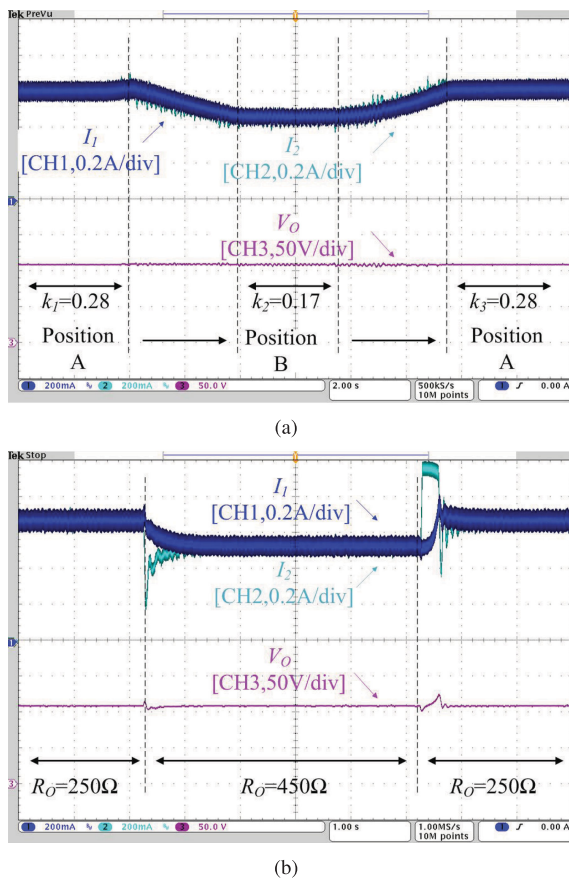

Fig. 13. Transient waveforms of I_1, I_2, and V_O for (a) k dynamically changing from $k_1 = 0.28$ (position A) to $k_2 = 0.17$ (position B) and from $k_2 = 0.17$ (position B) back to $k_1 = 0.28$ (position A), at the loading condition $R_O = 300\ \Omega$. (b) R_O step changing from 250 to 450 Ω and from 450 to 250 Ω at $k = 0.28$.

rectifier circuit of the IPT converter is kept lagging behind i_i with a phase angle of $\frac{\pi}{2}$.

Transient waveforms of I_1 and I_2 using a linear controller for dynamic variations of k and load are shown in Fig. 13(a) and (b), respectively. The efficiency of the system is kept at its optimized value by observing that the instantaneous currents I_1 and I_2 are kept almost identical. Using the PI controller, the steady-state error is almost eliminated. In comparison to the control of the SS IPT converter, the linear control for the PP IPT converter in this paper needs specifically more control loops for the input current and frequency tracking. Thus, the overall controller speed is slower.

VII. CONCLUSION

A general linear control scheme for all four basic IPT systems to track the optimum efficiency point and independently regulate the output power is proposed in this paper. To facilitate the control, an additional control of either frequency or adaptive compensation is identified and formulated for the SP, PS, and PP IPT converters against the variation of coupling coefficient (k). Control references of the k- and load-independent transfer functions are derived for all the four basic IPT converters for the fast linear control. The maximum efficiencies of four basic IPT systems are analyzed, compared, and verified theoretically and experimentally. It is found that the maximum efficiencies of the four basic IPT systems are in decreasing order given by PP, SP, PS, and SS compensated IPT converters. The linear control scheme with additional frequency control in conjunction with optimum efficiency tracking and independent load regulation is validated experimentally using an efficient PP IPT converter system.

REFERENCES

[1] S. Y. R. Hui, "Planar inductive battery charging system," U.S. Patent 7 576 514, Aug. 18, 2009.

[2] Y. Jang and M. M. Jovanovic, "A contactless electrical energy transmission system for portable-telephone battery chargers," *IEEE Trans. Ind. Electron.*, vol. 50, no. 3, pp. 520–527, Jun. 2003.

[3] B. Choi, J. Nho, H. Cha, T. Ahn, and S. Choi, "Design and implementation of low-profile contactless battery charger using planar printed circuit board windings as energy transfer device," *IEEE Trans. Ind. Electron.*, vol. 51, no. 1, pp. 148–157, Feb. 2004.

[4] Y. Yang, S. Tan, and S. Y. Hui, "Front-end parameter monitoring method based on two-layer adaptive differential evolution for SS-compensated wireless power transfer systems," *IEEE Trans. Ind. Inf.*, to be published, doi: 10.1109/TII.2019.2924926.

[5] J. M. Miller, P. T. Jones, J. M. Li, and O. C. Onar, "ORNL experience and challenges facing dynamic wireless power charging of EVs," *IEEE Circuits Syst. Mag.*, vol. 15, no. 2, pp. 40–53, May 2015.

[6] S. Zhou and C. Chris Mi, "Multi-paralleled LCC reactive power compensation networks and their tuning method for electric vehicle dynamic wireless charging," *IEEE Trans. Ind. Electron.*, vol. 63, no. 10, pp. 6546–6556, Oct. 2016.

[7] C. C. Mi, G. Buja, S. Y. Choi, and C. T. Rim, "Modern advances in wireless power transfer systems for roadway powered electric vehicles," *IEEE Trans. Ind. Electron.*, vol. 63, no. 10, pp. 6533–6545, Oct. 2016.

[8] Y. Li *et al.*, "A new coil structure and its optimization design with constant output voltage and constant output current for electric vehicle dynamic wireless charging," *IEEE Trans. Ind. Inf.*, to be published, doi: 10.1109/TII.2019.2896358.

[9] Y. Li *et al.*, "Reconfigurable intermediate resonant circuit based WPT system with load-independent constant output current and voltage for charging battery," *IEEE Trans. Power Electron.*, vol. 34, no. 3, pp. 1988–1992, Mar. 2019.

[10] Q. Chen, S. C. Wong, C. K. Tse, and X. Ruan, "Analysis, design, and control of a transcutaneous power regulator for artificial hearts," *IEEE Trans. Biomed. Circuits Syst.*, vol. 3, no. 1, pp. 23–31, Feb. 2009.

[11] H. Y. Leung, D. McCormick, D. M. Budgett, and A. P. Hu, "Pulse density modulated control patterns for inductively powered implantable devices based on energy injection control," *IET Power Electron.*, vol. 6, no. 6, pp. 1051–1057, Jul. 2013.

[12] S. C. Tang, T. L. T. Lun, Z. Guo, K. W. Kwok, and N. J. McDannold, "Intermediate range wireless power transfer with segmented coil transmitters for implantable heart pumps," *IEEE Trans. Power Electron.*, vol. 32, no. 5, pp. 3844–3857, May 2017.

[13] C. S. Wang, G. A. Covic, and O. H. Stielau, "Power transfer capability and bifurcation phenomena of loosely coupled inductive power transfer systems," *IEEE Trans. Ind. Electron.*, vol. 51, no. 1, pp. 148–157, Feb. 2004.

[14] N. A. Keeling, G. A. Covic, and J. T. Boys, "A unity-power-factor IPT pickup for high-power applications," *IEEE Trans. Ind. Electron.*, vol. 57, no. 2, pp. 744–751, Feb. 2010.

[15] W. Zhong and S. Y. Hui, "Reconfigurable wireless power transfer systems with high energy efficiency over wide load range," *IEEE Trans. Power Electron.*, vol. 33, no. 7, pp. 6379–6390, Jul. 2018.

[16] M. Fu, C. Ma, and X. Zhu, "A cascaded boost–buck converter for high-efficiency wireless power transfer systems," *IEEE Trans. Ind. Inform.*, vol. 10, no. 3, pp. 1972–1980, Aug. 2014.

[17] M. Fu, H. Yin, X. Zhu, and C. Ma, "Analysis and tracking of optimal load in wireless power transfer systems," *IEEE Trans. Power Electron.*, vol. 30, no. 7, pp. 3952–3963, Jul. 2015.

[18] H. Li, J. Li, K. Wang, W. Chen, and X. Yang, "A maximum efficiency point tracking control scheme for wireless power transfer systems using magnetic resonant coupling," *IEEE Trans. Power Electron.*, vol. 30, no. 7, pp. 3998–4008, Jul. 2015.

[19] W. X. Zhong and S. Y. R. Hui, "Maximum energy efficiency tracking for wireless power transfer systems," *IEEE Trans. Power Electron.*, vol. 30, no. 7, pp. 4025–4034, Jul. 2015.

[20] T. D. Yeo, D. Kwon, S. T. Khang, and J. W. Yu, "Design of maximum efficiency tracking control scheme for closed-loop wireless power charging system employing series resonant tank," *IEEE Trans. Power Electron.*, vol. 32, no. 1, pp. 471–478, Jan. 2017.

[21] Z. Li, C. Zhu, J. Jiang, K. Song, and G. Wei, "A 3-kW wireless power transfer system for sightseeing car supercapacitor charge," *IEEE Trans. Power Electron.*, vol. 32, no. 5, pp. 3301–3316, May 2017.

[22] Y. Yang, W. Zhong, S. Kiratipongvoot, S. C. Tan, and S. Y. R. Hui, "Dynamic improvement of series-series compensated wireless power transfer systems using discrete sliding mode control," *IEEE Trans. Power Electron.*, vol. 33, no. 7, pp. 6351–6360, Jul. 2018.

[23] D. Patil, M. Sirico, L. Gu, and B. Fahimi, "Maximum efficiency tracking in wireless power transfer for battery charger: Phase shift and frequency control," in *Proc. IEEE Energy Convers. Congr. Expo.*, 2016, pp. 1–8.

[24] Z. Huang, S. C. Wong, and C. K. Tse, "Control design for optimizing efficiency in inductive power transfer systems," *IEEE Trans. Power Electron.*, vol. 33, no. 5, pp. 4523–4534, May 2018.

[25] W. Zhang, S. C. Wong, C. K. Tse, and Q. Chen, "Analysis and comparison of secondary series and parallel compensated inductive power transfer systems operating for optimal efficiency and load-independent voltage-transfer ratio," *IEEE Trans. Power Electron.*, vol. 29, no. 6, pp. 2979–2990, Jun. 2014.

[26] W. Zhang, S. C. Wong, C. K. Tse, and Q. Chen, "Load-independent duality of current and voltage outputs of a series or parallel compensated inductive power transfer converter with optimized efficiency," *IEEE J. Emerg. Sel. Topics Power Electron.*, vol. 3, no. 1, pp. 137–146, Mar. 2015.

[27] K. C. A. Smith and R. E. Alley, *Electrical Circuit: An Introduction*. Cambridge, U.K.: Cambridge Univ. Press, 1992.

[28] S. Samanta and A. K. Rathore, "Analysis and design of load-independent ZPA operation for P/S, PS/S, P/SP, and PS/PS tank networks in IPT applications," *IEEE Trans. Power Electron.*, vol. 33, no. 8, pp. 6476–6482, Aug. 2018.

[29] E. Gati, G. Kampitsis, and S. Manias, "Variable frequency controller for inductive power transfer in dynamic conditions," *IEEE Trans. Ind. Electron.*, vol. 32, no. 2, pp. 1684–1696, Feb. 2017.

[30] L. Xu, Q. Chen, X. Ren, S. C. Wong, and C. K. Tse, "Self-oscillating resonant converter with contactless power transfer and integrated current sensing transformer," *IEEE Trans. Power Electron.*, vol. 32, no. 6, pp. 4839–4851, Jun. 2017.

[31] G. A. Covic, J. T. Boys, A. M. W. Tam, and J. C. H. Peng, "Self tuning pick-ups for inductive power transfer," in *Proc. IEEE Power Electron. Spec. Conf.*, 2008, pp. 3489–3494.

[32] T. C. Beh, M. Kato, T. Imura, S. Oh, and Y. Hori, "Automated impedance matching system for robust wireless power transfer via magnetic resonance coupling," *IEEE Trans. Ind. Electron.*, vol. 60, no. 9, pp. 3689–3698, Sep. 2013.

[33] A. Kamineni, G. A. Covic, and J. T. Boys, "Self-tuning power supply for inductive charging," *IEEE Trans. Ind. Electron.*, vol. 32, no. 5, pp. 3467–3479, May 2017.

[34] J. T. Boys and G. A. Covic, "The inductive power transfer story at the University of Auckland," *IEEE Circuits Syst. Mag.*, vol. 15, no. 2, pp. 6–27, Second Quarter 2015.

[35] D. Patil, M. Mcdonough, J. Miller, B. Fahimi, and P. T. Balsara, "Wireless power transfer for vehicular applications: Overview and challenges," *IEEE Trans. Transp. Electrif.*, vol. 4, no. 1, pp. 3–37, Mar. 2018.

Zhicong Huang (M'18) received the B.Eng. degree in electrical engineering and automation and the M.Phil. degree in mechanical and electronic engineering from the Huazhong University of Science and Technology, Wuhan, China, in 2010 and 2013, respectively, and the Ph.D. degree in power electronics from The Hong Kong Polytechnic University, Kowloon, Hong Kong, in 2018.

He is currently an Assistant Professor with the Shien-Ming Wu School of Intelligent Engineering, Guangzhou International Campus of South China University of Technology, Guangzhou, China. In 2019, he was a Postdoctoral Fellow under the UM Macao Talent Program, with the State Key Laboratory of Analog and Mixed-Signal VLSI, University of Macau, Macao, China. His research interests include power electronics and its applications.

Siu-Chung Wong (M'01–SM'09) received the B.Sc. degree in physics from the University of Hong Kong, Hong Kong, in 1986, the M.Phil. degree in electronics from the Chinese University of Hong Kong, Hong Kong, in 1989, and the Ph.D. degree from the University of Southampton, Southampton, U.K., in 1997.

He is currently an Associate Professor with the Department of Electronic and Information Engineering, The Hong Kong Polytechnic University, Hong Kong, where he conducts research in power electronics.

Dr. Wong is a member of the Electrical College, The Institution of Engineers, Australia. He is an Associate Editor of the IEEE TRANSACTIONS ON CIRCUITS AND SYSTEMS II, an Editor of the *Energy and Power Engineering Journal*, and a member of the Editorial Board of the *Journal of Electrical and Control Engineering*.

Chi K. Tse (M'90–SM'97–F'06) received the B.Eng. (Hons.) degree in electrical engineering and the Ph.D. degree from the University of Melbourne, Melbourne, VIC, Australia, in 1987 and 1991, respectively.

He is currently the Chair Professor of Electrical Engineering with the City University of Hong Kong, Kowloon, Hong Kong. Prior to joining City University of Hong Kong in October 2019, he was with The Hong Kong Polytechnic University, where he was the Head of the Department of Electronic and Information Engineering from 2005 to 2012. His research interests include power electronics, nonlinear circuits, and complex network applications.